Available online at www.sciencedirect.com
ScienceDirect
Tectonophysics 424 (2006) 351–366
TECTONOPHYSICS
www.elsevier.com/locate/tecto

Application of a modified pattern informatics method to forecasting the locations of future large earthquakes in the central Japan

K.Z. Nanjo [a,*], J.R. Holliday [b], C.-c. Chen [c], J.B. Rundle [b], D.L. Turcotte [d]

[a] The Institute of Statistical Mathematics, Minato-ku, Tokyo 106-8569, Japan
[b] Center for Computational Science and Engineering, University of California at Davis, One Shield Avenue, Davis, CA 95616, USA
[c] Department of Earth Sciences and Graduate Institute of Geophysics, National Central University, Jhongli, Taoyuan, Taiwan 320, ROC
[d] Department of Geology, University of California at Davis, One Shield Avenue, Davis, CA 95616, USA

Received 5 August 2005; received in revised form 1 December 2005; accepted 25 March 2006
Available online 19 June 2006

Abstract

We propose a modification of the Pattern Informatics (PI) method that has been developed for forecasting the locations of future large earthquakes. This forecast is based on analyzing the space–time patterns of past earthquakes to find possible locations where future large earthquakes are expected to occur. A characteristic of our modification is that the effect of errors in the locations of past earthquakes on the output forecast is reduced. We apply the modified and original methods to seismicity in the central part of Japan and compared the forecast performances. We also invoke the Relative Intensity (RI) of seismic activity and randomized catalogs to constitute null hypotheses. We do statistical tests using the Molchan and Relative Operating Characteristic (ROC) diagrams and the log-likelihoods and show that the forecast for using the modified PI method is generally better than the competing original-PI forecast and the forecasts from the null hypotheses. Using the bootstrap technique with Monte-Carlo simulations, we further confirm that earthquake sequences simulated based on the modified-PI forecast can be statistically the same as the real earthquake sequence so that the forecast is acceptable. The main and innovative science in this paper is the modification of the PI method and the demonstration of its applicability, showing a considerable promise as an intermediate-term earthquake forecasting tool.

Keywords: Patterns; Earthquakes; Earthquake prediction; Seismicity; Seismic quiescence

1. Introduction

The Earth's crust is clearly extremely complex and it is generally accepted that earthquakes are a chaotic phenomenon (Turcotte, 1997). Thus, as in the case of weather forecasting, earthquake forecasting must be considered on a statistical basis (Rundle et al., 2003). The statistical properties of seismicity patterns can be used to forecast future earthquakes. Basic types of statistical seismicity precursors include foreshock, quiescence, swarms, activation, and doughnuts (e.g., Mogi, 1985; Turcotte, 1991; Scholz, 2002; Kanamori, 2003). For example, a sequence of earthquakes preceded the 1906 San Francisco earthquakes (Sykes and Jaumè, 1990). This type of seismic activation has been reported and quantified as a power-law increase of the number of earthquakes with time prior to the large earthquake (e.g.,

* Corresponding author. Tel.: +81 3 3446 1501; fax: +81 3 5421 8796.
E-mail addresses: nanjo@ism.ac.jp, nanjo@cse.ucdavis.edu (K.Z. Nanjo).

0040-1951/$ - see front matter © 2006 Elsevier B.V. All rights reserved.
doi:10.1016/j.tecto.2006.03.043

Bufe and Varnes, 1993; Bowman et al., 1998; Jaumè and Sykes, 1999; Main, 1999). However, the success of these studies has depended on knowing the location of the subsequent earthquake. Several groups systematically developed algorithms to find premonitory seismicity patterns. The Russian group studied premonitory seismic activation for some strong earthquakes in California and Nevada using algorithm "CN" and for magnitude $m > 8$ worldwide using algorithm "M8" (e.g., Kellis-Borok, 1990; Kellis-Borok and Rotwain, 1990; Kellis-Borok and Kossobokov, 1990; Kellis-Borok and Soleviev, 2003). Another group (e.g., Wyss, 1997; Wyss and Martirosyan, 1998; Wyss and Wiemer, 2000) found premonitory seismic quiescence for Armenian and Landers earthquakes using algorithm "Zmap" (see also Wyss and Habermann, 1988). Independently from this group, Enescu and Ito (2001) used the algorithm and found premonitory quiescence before the 1995 Hyogo-Ken Nanbu (Kobe) earthquake. However, several researchers pointed out that some of these results lead to conflicting assessments of the algorithms' effectiveness (Matthews and Reasenberg, 1987; Rundle et al., 2003).

A new approach to earthquake forecasting, the Pattern Informatics (PI) approach, has been proposed by Rundle et al. (2002) and Tiampo et al. (2002). This approach is based on the strong space–time correlations that are responsible for the cooperative behavior of driven threshold systems and arises both from threshold dynamics as well as from the mean field (long range) nature of the interactions. The PI technique can be used to detect precursory seismic activation or quiescence and make earthquake forecasts. The PI method has been applied to California, Japan, and on a worldwide basis for forecasting large events during the period from 2000 to 2009 (Tiampo et al., 2002; Rundle et al., 2002, 2003; Holliday et al., 2005; Nanjo et al., in press), and we are still checking how this works. For example, our group made a forecast map for the central part of Japan. This map was first presented by one of the authors (JBR) at an invited lecture at Kyoto University, chaired by Prof. James Mori on October 13, 2004, and at the International Conference on Geodynamics held on Oct. 14–16, 2004 at the University of Tokyo, Japan (Organizer: Prof. Mitsuhiro Matsu'ura, University of Tokyo), prior to the occurrence of the Oct. 23, 2004 Niigata earthquake (magnitude of 6.8). This earthquake occurred very near the area where future large earthquakes were expected, but not on the area. This imperfect forecast suggests the requirement of improving the method for better earthquake forecasting. The purpose of this paper is to discuss a modification of the PI method and apply the modified method to the seismicity in the study region that Nanjo et al. (in press) considered. We test whether or not the forecast by using this new method is better than the forecast by using the original one and the forecasts from two null hypotheses. These hypotheses are based on the spatially coarse-grained Relative Intensity (RI) of seismic activity and on a set of randomized or reshuffled catalogs as in previous papers (e.g., Bowman et al., 1998; Zöller et al., 2001; Tiampo et al., 2002). For our test, we do visual comparison between the forecast maps generated by using both methods. We also use statistical examinations based on (1) the log-likelihood test, (2) the Molchan diagram (e.g., Molchan, 1997), (3) the Receiver (or Relative) Operating Characteristic (ROC) diagram (Joliffe and Stephenson, 2003), and (4) the bootstrap technique (e.g., Kagan and Jackson, 1994). The use of (1), (2), and (4) for the forecast verification has been proposed by many seismologists (e.g., Kagan and Jackson, 1995; Jackson, 1996; Gross and Rundle, 1998; Kagan and Jackson, 2000; Newman and Turcotte, 2002; Schorlemmer et al., 2006; McGuire et al., 2005). The ROC diagram has been used in the field of atmospheric sciences (Joliffe and Stephenson, 2003), and recently it was introduced to seismology (Holliday et al., 2005). We describe these four methods for forecast verification so that they can be reproducible. The modified method that we will present is one of the novel and innovative points in our paper. Note that Nanjo et al. (in press) did not use this type of modification. Before discussing the PI method and its modification, we will consider the null hypotheses invoked for our forecast verification.

2. Forecasting techniques

2.1. Null hypotheses

To establish forecast verification, the PI forecast must be better than other candidate forecasts from the null hypotheses. For this purpose, we use two kinds of forecasts. One is a forecast based on the coarse-grained Relative Intensity (RI) of seismicity. Measures similar to the RI forecast have been proposed for the "standard null hypothesis" (Kagan and Jackson, 2000). The RI hypothesis was used for testing the PI forecast for southern California earthquakes (Tiampo et al., 2002). An alternative candidate is a forecast based on a number of synthetic random catalogs or reshuffled catalogs. We denote this as RAN forecast. The use of this type of forecast has been proposed by many researchers (e.g., Bowman et al., 1998; Zöller et al., 2001; Tiampo et al.,

2002) to quantify the probability of successful forecasts to occur by chance. The reader can assess how more significant the PI forecast is against the RI one, because we really do not know how to quantify and how much to believe the observed better performance of PI. From a practical standpoint, such tests will be the only way to show the effectiveness of the proposed method. Before discussing the RAN forecast, we will consider the RI forecast.

1. The study region is divided into a grid of boxes. Each box has a linear dimension of Δx.
2. The number of earthquakes with magnitude m larger than or equal to a lower cutoff magnitude m_c in box i is determined during the period from t_S to t_E. This number is averaged to obtain the number of earthquakes per day, denoted by $n_i(t_S,t_E)$.
3. Relative value of this number is called RI score. This score is given in the form $n_i(t_S,t_E)/n_{MAX}$, where n_{MAX} is the largest value of $n_i(t_S,t_E)$. The RI score lies between zero and one.
4. If we consider a threshold value w in the interval from zero to one ($0 \le w \le 1$), future large earthquakes are expected only in boxes of RI scores larger than this value w. The boxes of RI scores smaller than the threshold value w are the sites at which future large earthquakes are forecast not to occur.
5. In the framework of RI forecast, larger earthquakes are considered most likely to occur at sites of higher seismic activity. This forecast constructs the first null hypothesis.

Although many researchers (e.g., Bowman et al., 1998; Zöller et al., 2001) proposed algorithms to make a synthetic random catalog or reshuffled catalog, we use a similar procedure taken by Tiampo et al. (2002). Note that the concept of their randomizing technique is similar to that used by Bowman et al. (1998) and Zöller et al. (2001). To construct a random earthquake catalog, we take the number of earthquakes in this catalog to be the same as that of earthquakes in the real catalog. For an event, we assign an occurrence time at random over the years t_S to t_E. We also randomly assign locations over the study region. Events assigned by this process constitute a catalog. Randomizing in this way destroys whatever coherent space–time structure may have existed in the data. We apply the modified PI method that will be introduced in Section 2.2 to a set of the random catalogs obtained by this procedure. This application constructs the second null hypothesis. The approach based on this hypothesis is the RAN forecast.

2.2. PI method and its modification

We give a brief description of the original PI method and then discuss its modification.

1. As was done for the RI forecast, the study region is divided into a grid of boxes with a linear dimension Δx.
2. All earthquakes in the region with $m \ge m_c$ since the time denoted by t_0 are included. Note that aftershocks are not removed from our analysis. Our method is based on the strong space–time correlations that are responsible for the cooperative behavior of earthquakes and aftershocks are also considered to constitute an important component of the correlations.
3. Three time intervals are considered.
   i). A reference time interval from t_b to t_1.
   ii). A second time interval from t_b to t_2 ($t_2 > t_1$). The change interval over which seismic activity changes are computed is then from t_1 to t_2. The time t_b is chosen to lie between t_0 and t_1. The objective is to quantify anomalous seismic activity in the change interval from t_1 to t_2 relative to the reference interval from t_b to t_1.
   iii). The forecast time interval from t_2 to t_3 is the interval for which the forecast is valid. We take the change and forecast interval to have the same length.
4. The seismic intensity of a box for time interval is the average number of earthquake with $m \ge m_c$ that occurred during the time interval. The seismic intensity of box i over the reference interval t_b to t_1, $n_i(t_b,t_1)$, is the average number of earthquakes from t_b to t_1. The seismic intensity of box i over the interval t_b to t_2, $n_i(t_b,t_2)$, is the average number of earthquakes from t_b to t_2.
5. In order to compare the intensities from two different time intervals, we require that they have the same statistical properties. Therefore, we normalize the seismic intensities by subtracting the mean seismic activity of all boxes and dividing by the standard deviation of the seismic activity in all boxes. We denote these normalized intensities by $n_i^*(t_b,t_1)$ and $n_i^*(t_b,t_2)$.
6. Our measure of anomalous seismicity in box i is the difference between the two normalized seismic intensities, $\Delta n_i^*(t_b,t_1,t_2) = n_i^*(t_b,t_2) - n_i^*(t_b,t_1)$.
7. To reduce the relative importance of random fluctuations (noise) in seismic activity, we

compute the average change $\Delta n_i^*(t_b,t_1,t_2)$ over all possible initial times t_b from t_0 to t_1. The result is $\Delta \underline{n_i^*}(t_0,t_1,t_2)$.

8. We define the probability of a future earthquake in box i, $P_i(t_0,t_1,t_2)$, as the square of the average intensity change, $P_i(t_0,t_1,t_2)=\{\Delta \underline{n_i^*}(t_0,t_1,t_2)\}^2$.
9. To identify anomalous regions, we wish to compute the change in the probability $P_i(t_0,t_1,t_2)$ relative to the background so that we subtract the mean probability over all boxes $<P_i(t_0,t_1,t_2)>$. This change in the probability is denoted by $P_i'(t_0,t_1,t_2)=P_i(t_0,t_1,t_2)-<P_i(t_0,t_1,t_2)>$.
10. Relative value of the change in the probability is called the PI score. This score is given in the form $P_i'(t_0,t_1,t_2)/P_{MAX}$, where P_{MAX} is the largest value of $P_i'(t_0,t_1,t_2)$. Because we are interested in seismic activation and seismic quiescence relative to the background, if boxes have the PI scores smaller than zero, these scores are replaced by zero. The PI score is zero to one.
11. If we consider a threshold value w in the interval from zero to one, future large earthquakes are expected likely in boxes of PI scores larger than this value w. The boxes of PI scores smaller than the threshold value w are the sites at which future large earthquakes are forecast not to occur.
12. In the framework of PI forecast, larger earthquakes are considered likely to occur at sites of higher seismic activity or quiescence.

The original procedure described above was used to construct a forecast for California (Tiampo et al., 2002, Rundle et al., 2002, 2003; Holliday et al., 2005). Also, this method was used in our preliminary research (Nanjo et al., in press) for the same study region that we consider in this paper. Here we introduce a modification of the PI method. This modification is to use a Moore neighborhood for the process of binning the data, thereby accounting for errors in event location. The Moore-binning is implemented by averaging the seismicity over the box and the 8 surrounding boxes (the Moore neighborhood is discussed in Wolfram, 2002). We count the total number of earthquakes in box i and the 8 surrounding boxes for the reference interval from t_b to t_1. Then, this number is divided by 9, and we regard this divided number as the number of earthquakes associated with box i for the reference interval. This modification for obtaining the seismic intensity $n_i(t_b,t_1)$ replaces step 4 of the original PI method. This number is averaged over the reference interval to obtain $n_i(t_b,t_1)$. This process of binning data is applied to obtain the other intensity $n_i(t_b,t_2)$ as well as the intensity $n_i(t_S,t_E)$ in step 2 of the RI method. Note that this modification was not used by Nanjo et al. (in press). We will compare the forecast map generated by using the original method shown in Nanjo et al. (in press) with that by using the modified method.

3. Methods for forecast verification

3.1. ROC and Molchan diagrams

In this framework of ROC, meteorological phenomena such as tornadoes, rains, and floods can be regarded as simple binary events and forecasts for these events are often issued as unqualified states that they are or are not likely to occur. This type of forecasts is referred to as yes/no or binary forecast. The ROC diagram is based on a 2×2 contingency table. As done for tornado forecasts by Joliffe and Stephenson (2003), let us consider this table for earthquake forecasts. The contingency table is constructed as follows: The top left cell represents the number of boxes (a) where earthquakes had been forecast to occur ($s\geq w$) and earthquakes were actually observed. Either PI score or RI score is denoted by s. The top right cell represents the number of boxes (b) where earthquakes had been forecast to occur ($s\geq w$) but no earthquakes were observed. The bottom left cell represents the number of boxes (c) where earthquakes had been forecast not to occur ($s\leq w$) but earthquakes were actually observed. The bottom right cell represents the number of boxes (d) where earthquakes had been forecast not to occur ($s\leq w$) and no earthquakes were actually observed. Following Joliffe and Stephenson (2003), this table provides us with hit rate $H_{ROC}=a/(a+c)$ and false alarm rate $F=b/(b+d)$. These rates are in the range from zero to one. The ROC diagram is based on the hit rate H_{ROC} against the false alarm rate F. As the decision threshold w varies from low to high, the values of H_{ROC} and F vary together from high to low to trace out the ROC curve for the system. A benchmark forecast is an ideal random forecast (RAN forecast), expressed by the equation $H_{ROC}=F$ (Joliffe and Stephenson, 2003). A better forecast is located in the upper left relative to the equation. The perfect forecast is represented by an ROC that rises from $(F, H_{ROC})=(0, 0)$ along the H_{ROC}-axis to (0, 1), then straight to (1, 1). Holliday et al. (2005) applied the diagram to verify their forecast skill for California earthquakes. However, the direct application of this diagram to Japan seems to be not appropriate. As shown later, we see strong clustering of seismicity such as earthquake swarms and aftershock sequences in the study region. Within the framework of the original ROC diagram, we do not consider the total number of

earthquakes forecast to occur in each box, rather we ask only whether at least one earthquake occurs at a forecast location. As a result, the effect of clustering cannot be easily evaluated for this method of forecast verification. Here we consider a case given below to modify the original ROC diagram: all earthquakes that land on one box are considered separately. We compute the contingency table according to the following recipe. Suppose that there are, say 50 earthquakes in the forecast interval. Then, assume that some of these hit the same box. We consider $J=50$ earthquakes to constitute 50 independent realizations of the test. For each realization, we compute a contingency table given in Table 1a. The q-th realization is computed as follows: a_q is defined by the number (either 1 or 0) of boxes with $s \geq w$ hit by the one earthquake during the forecast interval; b_q is defined by the number of boxes with $s \geq w$ not hit by the earthquake during the forecast interval; c_q is defined by the number (either 1 or 0) of boxes with $w \geq s \geq 0$ hit by the earthquake during the forecast interval; and d_q is defined by the number of boxes with $w \geq s \geq 0$ not hit by the earthquake during the forecast interval. In this example, there will be $J=50$ such contingency tables. To obtain the total contingency table, we compute to individually sum a_q, b_q, c_q, and d_q, as shown in Table 1b.

The Molchan diagram has been used for earthquake prediction as a decision-making problem (e.g., Molchan, 1997; Newman and Turcotte, 2002; McGuire et al., 2005). This diagram is based on the hit rate H_{MOL} and the alarm rate r. We divide the number of earthquakes that occurred at boxes where earthquakes were forecast to occur ($s \geq w$) by the total number of earthquakes to be forecasted. This divided number defines the hit rate H_{MOL}. We next divide the number of boxes where earthquakes had been forecast to occur ($s \geq w$) by the total number of boxes. This divided number defines the alarm rate r. As done for the ROC diagram, the decision threshold w varies from low to high so that the values of H_{MOL} and r vary together from high to low to trace out the Molchan curve for the system. Similarly to the ROC, the equation $H_{\mathrm{MOL}}=r$ is a benchmark forecast, an ideal random forecast (RAN forecast). A better forecast is located in the upper left relative to the equation.

Table 1
Nomenclature of contingency tables for the ROC diagram

Forecast	Observed		
	Yes	No	Total
a			
Yes	a_q	b_q	a_q+b_q
No	c_q	d_q	c_q+d_q
Total	a_q+c_q	b_q+d_q	$a_q+b_q+c_q+d_q$
b			
Yes	$a_{\mathrm{SUM}}=\sum_{q=1}^{50}a_q$	$b_{\mathrm{SUM}}=\sum_{q=1}^{50}b_q$	$a_{\mathrm{SUM}}+b_{\mathrm{SUM}}$
No	$c_{\mathrm{SUM}}=\sum_{q=1}^{50}c_q$	$d_{\mathrm{SUM}}=\sum_{q=1}^{50}d_q$	$c_{\mathrm{SUM}}+d_{\mathrm{SUM}}$
Total	$a_{\mathrm{SUM}}+c_{\mathrm{SUM}}$	$b_{\mathrm{SUM}}+d_{\mathrm{SUM}}$	$a_{\mathrm{SUM}}+b_{\mathrm{SUM}}+c_{\mathrm{SUM}}+d_{\mathrm{SUM}}$

(a) The contingency table for the q-th realization. (b) The total contingency table.

3.2. Likelihood test

The likelihood test is used to evaluate the accuracy with which the score s can forecast future ($t_2<t\leq t_3$) large ($m_{\mathrm{JMA}}\geq 5$) events, relative to forecasts from the null hypotheses. The likelihood L is a probability measure that can be used to assess the utility of one forecast measure over another. Typically, one computes the logarithm of the likelihood ($\log_{10}L$) for the proposed measure and compares this measure to the likelihood measure for a representative null hypothesis. The ratio of these two values then yields information about which measure is more accurate in forecasting future events.

In the likelihood test, a probability density function is required. We use a global Gaussian model and a local Poissonian model. The use of the Gaussian model was proposed for testing the PI method forecast (Tiampo et al., 2002). The second model used is based on work performed by the Regional Earthquake Likelihood Methods (RELM) group (Schorlemmer et al., 2006). The likelihood is defined by L_{G} for the Gaussian model and by L_{P} for the Poissonian model.

3.2.1. Global Gaussian model

In their original analysis, Tiampo et al. (2002) calculated likelihood values by defining $Pr[x]$ to be the union of a set of N Gaussian density functions p_{G} ($|x-x_i|$) (Bevington and Robinson, 1992) centered at each box x_i. Each individual Gaussian has a standard deviation σ equal to the box scale Δx ($0.1\approx 10$ km in this study) and a peak value equal to the calculated score s_i (PI score, RI score or RAN score at box i) divided by σ^2. $Pr[x(e_j)]$ is therefore a probability measure that the j-th future large earthquake e_j occurs at location $x(e_j)$,

$$Pr[x(e_j)] = \sum_{i=1}^{N} \frac{s_i}{\sigma^2} \exp\left[-\frac{|x(e_j)-x_i|^2}{\sigma^2}\right]. \quad (1)$$

If there are J future events, the likelihood L_{G} that all J events are forecast is

$$L_{\mathrm{G}} = \prod_{j=1}^{J} \frac{Pr[x(e_j)]}{\sum_{i=1}^{N} Pr[x_i]}. \quad (2)$$

We consider the ten-based logarithm of this value L_G, $\log_{10}(L_G)$.

3.2.2. Local Poissonian model

Following Schorlemmer et al. (2006), the second model used is introduced. For each box i, an expectation value ζ_i is calculated by scaling the local score s_i by the number of earthquakes that occurred over all space during the forecasted time period,

$$\zeta_i = \theta s_i, \tag{3}$$

where θ is the number of post-t_2 events. Note that for any future time interval ($t_2<t<t_3$), θ could in principle be estimated by using the Gutenberg–Richter relation. For each box an observation value ω_i is also calculated such that ω_i contains the number of post-t_2 earthquakes that actually occurred in box i. Note that $\sum_{i=1}^{N} \omega_i = \theta$. For this model it is assumed that earthquakes are independent of each other. Thus, the probability of observing ω_i events in box i with expectation ζ_i is the Poissonian probability,

$$p_i(\omega_i|\zeta_i) = \frac{\zeta_i^{\omega_i}}{\omega_i!}\exp(-\zeta_i). \tag{4}$$

The likelihood L_P for a given calculation is given by the product of the individual box probabilities,

$$L_P = \prod_{i=1}^{N} p_i(\omega_i|\zeta_i). \tag{5}$$

As was done for the Gaussian case, we take $\log_{10}(L_P)$ in order to evaluate a forecast skill.

It should be remarked that one of the known problems with likelihood method is that the computed likelihood score is strongly influenced by the probability value of the least-likely events. This problem means that assumptions about residual or "background probabilities" can determine the outcome of the test, especially when testing a model against a null hypothesis. Nonetheless, we use this likelihood because it is a standard practice for forecast verification in seismology.

4. Data and parameters

We use the data catalog maintained by the Japan Meteorological Agency (JMA). This catalog includes the data of earthquakes with $m_{JMA} \geq 0$ for the time period since 1923 in and around Japan. The relevant data consist of time, magnitude, and location given by east longitude, north latitude, and depth.

It is well known that the specific catalogue has one serious weakness, namely the m_{JMA} magnitude that it reports. A simple examination of m_{JMA} with moment magnitude, m_W, shows a very complicated behavior for the whole m_W ranges. A typical example for the m_{JMA} behavior is given by Scordilis (2005), where m_{JMA} breaks at $m_W=5.5$. Above this magnitude of $m_W=5.5$, m_{JMA} is roughly equal to m_W. Below $m_W=5.5$, m_{JMA} is smaller than m_W. As a result, $m_{JMA}=3.0$ means an $m_W=4.0$. This non-linear behavior simply creates a complex situation which is very different from California. However, we do not take care of the non-linear behavior between m_{JMA} and m_W because this choice does not influence our results. Our reason of the choice is that to generate forecast maps made by the use of PI and RI methods we consider the number of earthquakes in each box, not magnitude of earthquakes.

Study region is the region between 136.0–142.0° east longitude and between 33.0–38.0° north latitude, with the depth shallower than 20 km. This depth of 20 km is believed to be the lower limit of the crustal seismogenic zone in the study area, but does not include seismicity from the subduction zones. The Tokyo metropolitan area is located at the center of this region. We use $\Delta x=0.1° \approx 10$ km. Boxes of this size correspond roughly to the linear scale size of a $m_{JMA}=m_W \approx 5.6$–5.7 earthquake (Wells and Coppersmith, 1994). However, a $m_{JMA} \approx 5$ earthquake occurring within a box is large enough to influence the stress and seismicity within the entire box.

The study region is divided into a grid of 3000 square boxes of $0.1° \times 0.1° \times 20$ km. We try to forecast earthquakes of $m_{JMA} \geq 5$. The idea is to use information on small events having spatial scales $\lambda < \Delta x$ to forecast the occurrence of large events having scales $\lambda > \Delta x$. The question is what happens for events that are much larger than an event of magnitude $m_{JMA}>5$, for example $m_{JMA}=6.5$ or 7.0 events, which are almost annually found in Japan. One of the representative events is the Niigata earthquake ($m_{JMA}=6.8$) which has an expected fault length of more than 40 km, the scale of this is larger than the linear scale of four boxes. Our algorithm equally works between an event of $m_{JMA}=5$ and that of $m_{JMA}=6.5$ or 7.0. This means that the algorithm does not distinguish between them before the subsequent earthquake. In other words, we do not forecast the magnitude of expected earthquakes from the PI score.

The forecast of our algorithm is evaluated based on the epicentral location of an earthquake, not on the rupture area of the earthquake, irrespective of the magnitude. Although published work for quiescence patterns (e.g., Wyss, 1997; Wyss and Martirosyan, 1998; Wyss and Wiemer, 2000) indicated that these patterns were found to be close to the fault of the expected main

shock, seismic activation–acceleration is found on much larger space–scales of the order of 10 times the fault length (Sykes and Jaumè, 1990; Bufe and Varnes, 1993; Bowman et al., 1998; Jaumè and Sykes, 1999; Main, 1999; Du and Sykes, 2001). For example, Du and Sykes (2001) demonstrated that such pattern is found at some distance (similar to Mogi doughnut) from the epicenter. The space–scale of the activation–acceleration patterns is clearly larger than that of the premonitory patterns we consider. In future research, we will consider how the large-scale patterns previously reported are compatible with our analysis of seismic anomalies at scales of the order of the fault length.

We discuss the selection of the minimum magnitude m_c used for our analysis. Work on accelerated deformation (power-law increase on much larger space–scale) supports the conclusion that earthquakes to be used in the analysis should be taken as smaller by 2 magnitude units than the main shock (Bufe and Varnes, 1993). Jaumè and Sykes (1999) suggested 2–3 magnitude units and Papazachos et al. (2005) suggested a variation of this unit with the values between 1.5 and 2.0. This magnitude unit is not well constrained and in any case the studies on the accelerated deformation concern very different areas, but the typical value is 2. However, similar results do not exist for quiescence patterns. Tiampo et al. (2002), Rundle et al. (2002, 2003), and Holliday et al. (2005) applied the PI method to forecasting California earthquakes of magnitudes larger than or equal to 5, taking m_c to be 3. Their approach is to find both seismic activation and quiescence. Although m_c is not well constrained at this moment, we take into consideration the suggestions by Bufe and Varnes (1993), Jaumè and Sykes (1999), and Papazachos et al. (2005) and follow Tiampo et al. (2002), Rundle et al. (2002, 2003), and Holliday et al. (2005). We hypothesize that earthquakes with magnitudes larger than m_c+2 will preferentially occur following the anomaly during the forecast interval t_2 to t_3. However, we point out that it is of interest to test different values of m_c because this test might address how important the 2 magnitude units is for pattern identification, and would also allow for a magnitude-dependent performance investigation.

The reader may note that we do not remove aftershocks from our analysis. The use of the strong correlations in space–time domain that are responsible for the corporative behavior of earthquake is the basis of our method, and we believe that aftershocks constitute some parts of the correlations.

For the study region, we take the time t_0=Jan. 1, 1965 as a reference. The reader may note that the JMA catalog is not complete for earthquakes with magnitudes $m_{JMA} \geq 3$ since 1965. However, main question related to this time is whether the spatial pattern of the anomalies in the PI map is substantially changed for varying the time t_0. To address this question, the time t_0 will be taken to be in the range Jan. 1, 1940 to Jan. 1, 1988 to generate the modified PI forecast maps, then these maps are compared with the PI forecast map generated for the time t_0=Jan. 1, 1965. We do not see large differences among these maps for t_0=1940–1970. Therefore, we consider the reference time of t_0=Jan. 1, 1965. Details of the choice of this time will be discussed in Section 8.

The forecast interval is defined as ten years from Jan. 1, 2000 to Dec. 31, 2009. To forecast events in this interval, we use the change interval of ten years from Jan. 1, 1990 to Dec. 31, 1999. The length of the change interval is taken to be equal to that of the forecast interval. This equality is based on the implication from the diffusive mean field nature of the dynamics studied by Rundle et al. (2002) and Tiampo et al. (2002). See these papers for further detail. Forecasts computed from changes over a time interval $\Delta t = t_2 - t_1$ should convey information for time approximately in the range $t_2 < t \leq t_2 + \Delta t$. That is, the time interval Δt during which the change occur should be roughly the time interval Δt after t_2 for which the forecast is valid. Because of this, we take the length of the change interval to be equal to that of the forecast interval. Thus, our resulting maps that we will show are applicable to ≤ten-year forecasts but it is doubtful to apply these maps to >ten-year forecasts.

We now describe the large earthquakes that occurred in the study region during the forecast period. Ninety-seven earthquakes having $m_{JMA} \geq 5$ were observed during the period Jan. 1, 2000–the present. An earthquake swarm associated with Miyake volcano started on Jun. 26, 2000. Since then there have been 74 earthquakes with $5.0 \leq m_{JMA} < 6.0$ and six earthquakes with $6.0 \leq m_{JMA}$. This swarm is located at about 33.8–34.3° north latitude and 139.0–139.5° east longitude. The Oct. 23, 2004 Niigata Chuetsu earthquake of m_{JMA}=6.8 occurred. The epicentre was 138.7° east longitude and 37.3° north latitude and the depth was 6 km. Large aftershocks with $5.0 \leq m_{JMA}$ occurred around the hypocenter of this earthquake.

Finally, the times (t_S, t_E, t_0, t_1, t_2, t_3) and time intervals are summarized. The forecast interval is from Jan. 1, 2000 to Dec. 31, 2009. The change interval is from Jan. 1, 1990 to Jan. 1, 1999. The times are t_3=Dec. 31, 2009, $t_E = t_2$=Dec. 31, 1999, t_1=Jan. 1, 1990, and $t_S = t_0$=Jan. 1, 1965. Fig. 1a shows the spatial distribution of earthquakes (triangles) with magnitude $m_{JMA} \geq m_c$=3 during the period from $t_S = t_0$ to $t_E = t_2$. Circles are earthquakes with $m_{JMA} \geq 5$ since $t_E = t_2$.

5. Results

5.1. Forecast maps

The application of the original PI method was illustrated for the forecast period 2000–2009 by Nanjo et al. (in press) and is reproduced in Fig. 1b. Using the modified PI method, we generate the map for the same forecast period in Fig. 1c. PI scores are given in the form $\log_{10}$(PI score), using the color-code. A value of −4 corresponds, according to the color bar, to white color. However, note that physically, the white boxes actually

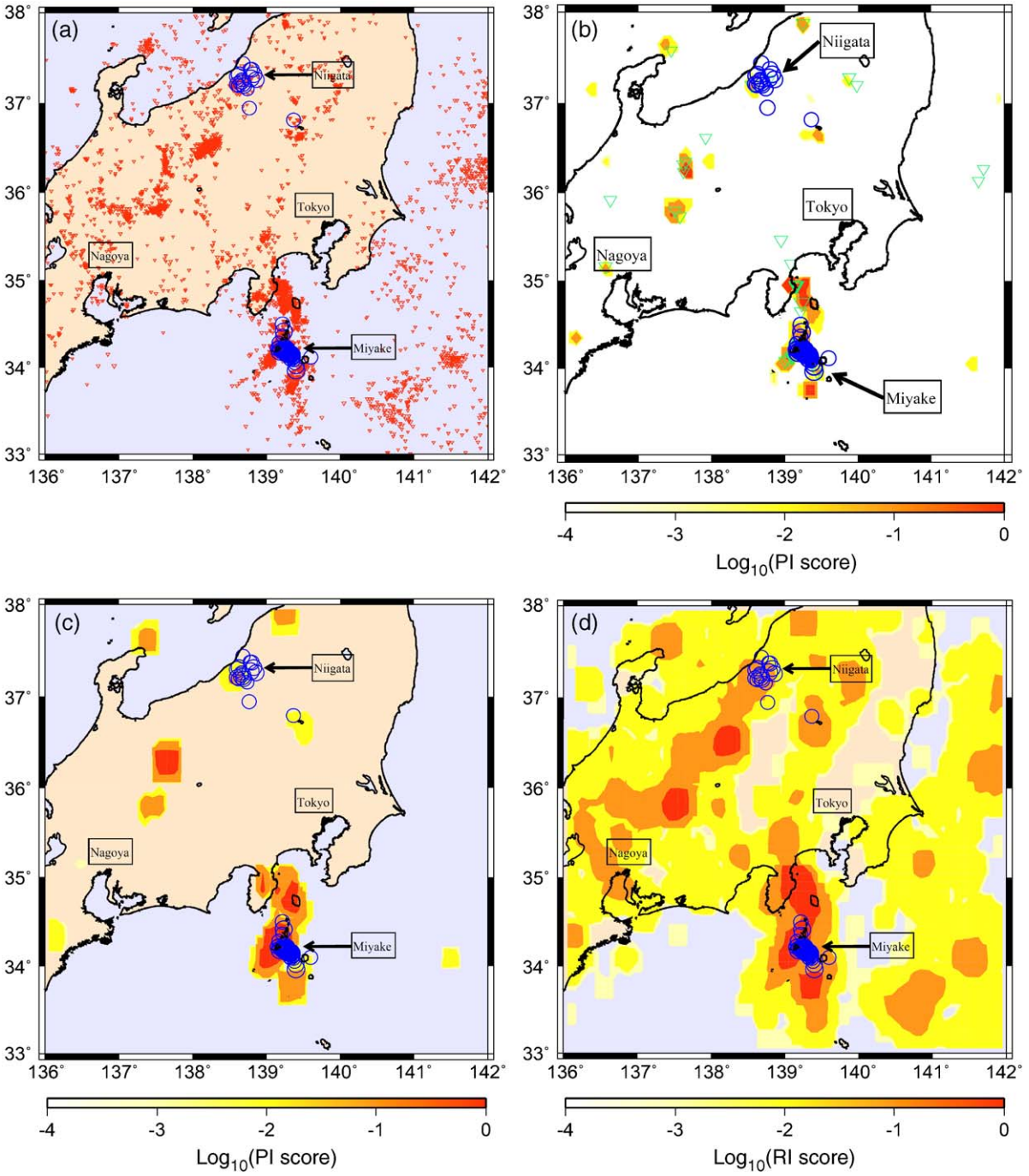

correspond to areas whose mean squared activity is equal to or less than the average of the entire region. Also note that the color bar is drawn with interpolated colors while in the figures only 4 discrete shades are found. Thus, based on the color bar, we know the approximate ranges of PI score for the individual map boxes in the figures. In the terminology of binary forecast maps, these discrete colors correspond to values of the "decision threshold" w (Joliffe and Stephenson, 2003). Further, note that coloring the onshore and offshore regions in eggshell does not give any information on the PI score. Only positive values of PI score are given so that the color-coded areas represent the areas of anomalously high seismic activation or quiescence relative to the mean level of activity. Circles for both figures are earthquakes with $m_{\mathrm{JMA}} \geq 5$ for the forecast interval. Triangles in Fig. 1b are earthquakes with $m_{\mathrm{JMA}} \geq 5$ within the change interval. In general, the color-coded anomalies are associated with future large earthquakes (circles). For example, circles for the 2000 Miyake earthquake swarm fall into the colored regions. The 2004 Niigata Chuetsu earthquake and its aftershocks did not occur at the seismically anomalous region, but near the region. Comparison between these figures shows that the association of the future large earthquakes with the color-coded anomalies in Fig. 1c is stronger than that in Fig. 1b. The modified approach in Fig. 1c enlarges the areas with high PI values and reduces "noisy" anomalies that are the areas with small PI values. Thus, our visual inspection prefers the modified PI method to the original one.

The application of the modified RI forecast (the use of the Moore neighborhood) is illustrated in Fig. 1d for the forecast period 2000–2009. The logarithmic values of the RI score, $\log_{10}$(RI score), are color-coded and this code is the same as that in Fig. 1b and c. Circles represent future large earthquakes. The procedure to make this map is the same as that to make the maps by using the original RI method in previous studies (Tiampo et al., 2002; Rundle et al., 2002, 2003) except for the use of a Moore neighborhood. Note that these circles are associated with the areas of large and moderate RI scores. Clearly, the possible locations where future large earthquakes are expected are broader than those in Fig. 1b and c.

Table 2
Hit rate H_{MOL} and alarm rate r of the modified PI and RI forecasts for $w=0.9$ (a) and $w=0.25$ (b)

a			b		
$w=0.9$	Hit rate, H_{MOL}	Alarm rate, r	$w=0.25$	Hit rate, H_{MOL}	Alarm rate, r
PI	51/97 =0.53	12/3000 =0.004	PI	78/97 =0.80	46/3000 =0.015
RI	0/97=0	16/3000 =0.005	RI	49/97 =0.51	60/3000 =0.02

5.2. Forecast verification

A rigorous test for forecast verification is needed, one whose underlying assumptions are understood, and whose performance has been evaluated extensively in the literature. We first consider the Molchan diagram. To make this diagram easily reproducible, we show the hit rate H_{MOL} and alarm rate r at two threshold values $w=0.9$ and 0.25 in Table 2 for the modified PI method (Fig. 1c) and the modified RI method (Fig. 1d). Varying the threshold from 1 to 0, we obtain many sets of H_{MOL} and r. Solid and dashed curves in red in Fig. 2a are the modified PI and RI forecasts, respectively. Table 2a is given by filled and unfilled triangles. Filled and unfilled circles give Table 2b. Also included are the results for the use of the original PI (blue solid curve) and RI (blue dashed curve) methods. Green line is the ideal RAN forecast ($H_{\mathrm{MOL}}=r$). Included in this figure is the RAN forecast based on 100 reshuffled catalogs (dash-dotted curves). In general, it can be seen that the modified PI approach (red solid curve) outperforms the original PI approach and the original and modified RI ones under

Fig. 1. Spatial distribution of earthquakes and forecast maps. (a) Epicenter map of earthquakes. The PI method forecast for the period 2000–2009, using (b) the original method and (c) the modified method. (d) The modified-RI-based forecast for the period 2000–2009. The times used are $t_0=t_{\mathrm{S}}=$Jan. 1, 1965, $t_1=$Jan. 1, 1990, and $t_2=t_{\mathrm{E}}=$Dec. 31, 1999. Circles represent events with $5.0 \leq m_{\mathrm{JMA}}$ during the time period 2000–the present. Geographic references (city names and name of earthquakes shown) are included into (a), (b), (c) and (d). Red triangles in (a) are the earthquakes of magnitude $m_{\mathrm{JMA}} \geq m_{\mathrm{c}}=3$ with the depth shallower than 20 km during the period from Jan. 1, 1965 to Dec. 31, 1999. Triangles in (b) are the earthquakes with $5.0 \leq m_{\mathrm{JMA}}$ in 1990–1999. The map in (b) is the same as that presented in Nanjo et al. (in press) but we include the geographic references into this figure. Logarithmic values of the PI score $\log_{10}$(PI score) in (b) and (c) and the RI score $\log_{10}$(RI score) in (d) are given using the color code. A value of −4 corresponds, according to the color bar, to white color, but note that this value corresponds to a transparency patch. Also note that the color bar is drawn with interpolated colors while in the figures only 4 discrete shades are existent. Thus, based on the color bar, we know approximate ranges of PI and RI scores for the individual colors in the figures. In the terminology of binary forecast maps, these discrete colors correspond to values of the "decision threshold" w (Joliffe and Stephenson, 2003). Further, note that coloring the onshore and offshore regions in eggshell does not give any information on the PI and RI scores.

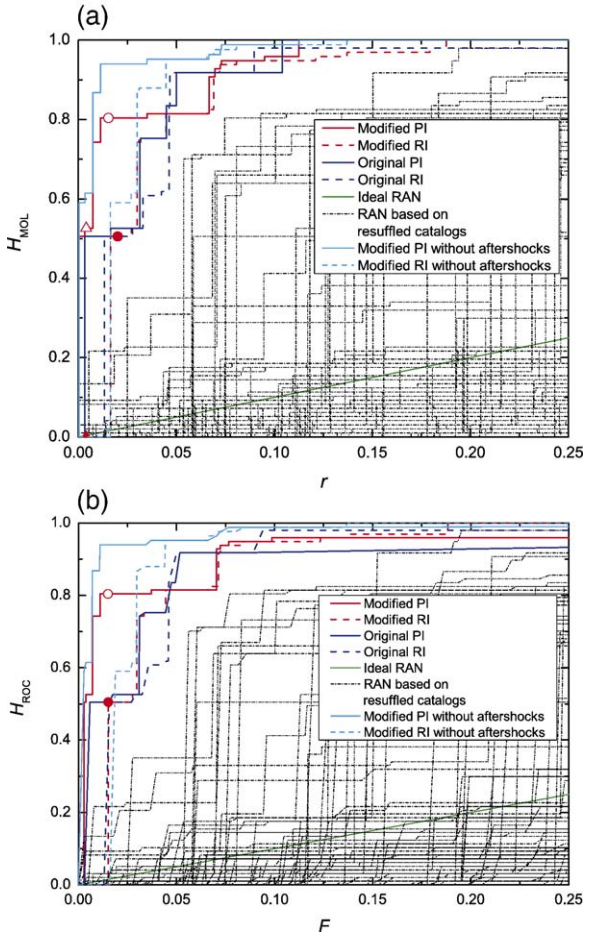

Fig. 2. Results of earthquake forecasts using the modified and original PI and RI methods based on Molchan diagram (a) and ROC diagram (b). Solid and dashed lines in red denote the results with the use of the modified PI and RI forecast, respectively. These lines in blue correspond to the original PI and RI forecasts, respectively. The ideal RAN forecast is expressed by the equations $H_{MOL}=r$ (a) and $H_{ROC}=F$ (b). The results of RAN forecasts obtained for 100 random catalogs are shown by the dash-dotted lines. Also included are the results of forecasting earthquakes without aftershocks of the Niigata earthquake by using the modified PI and RI methods (solid and dashed lines in cyan). For both figures, the filled circle (modified RI method) and the unfilled one (modified PI method) are associated with the threshold $w=0.25$. The filled triangle (modified RI method) and the unfilled one (modified PI method) in (a) correspond to the threshold $w=0.90$.

many circumstances and these approaches outperform the two RAN ones by a large margin.

We next take the ROC diagram. In order for the reader to reproduce what we did and judge whether our claims of successful forecasts are justified by the data or not, we show two contingency tables at a threshold value $w=0.25$ in Table 3 for the modified PI method (Fig. 1c) and the modified RI method (Fig. 1d). For this threshold, $H_{ROC}=78/97=0.804$ and $F=4384/290903=0.01507$ for the modified PI forecast and $H_{ROC}=49/97=0.505$ and $F=4413/290903=0.0151$ for the modified RI forecast. We obtain the values of H_{MOL} and r by varying the threshold from 1 to 0. Solid and dashed curves in red in Fig. 2b are the modified PI and RI forecasts, respectively. Filled and unfilled circles give Table 3. Also included are the results for the use of the original PI (blue solid curve) and RI (blue dashed curve) methods. Green line is the ideal RAN forecast ($H_{MOL}=r$) and dash-dotted curves are the RAN forecast based on 100 reshuffled catalogs. The results obtained here is consistent with those obtained for the Molchan diagram.

In the framework of ROC diagram, the values of a and c are very small, relative to those of b and d for all the values of the threshold w (a, $c<b$, d for all w). The area with false alarm is similar to the total alarm area. That is, the values of r are similar to those of F for many thresholds w. This is the reason why the diagram in Fig. 2a is very similar to that in Fig. 2b.

Next, we applied the likelihood test to competing the original and modified PI and RI forecasts. We first take the global Gaussian model. Then we compute the log-likelihoods: $\log_{10}(L_G)=-275$ for the original PI, $\log_{10}(L_G)=-296$ for the original RI, $\log_{10}(L_G)=-182$ for the modified PI, and $\log_{10}(L_G)=-249$ for the modified RI, and give them in Fig. 3a. Also included is the histogram of the log-likelihoods of RAN forecasts for applying the modified PI method to the 100 reshuffled catalogs. The log-likelihood $\log_{10}(L_G)=-182$ for the modified PI is larger than the others. Next we take the local Poissonian model. As for the global Gaussian model, the log-likelihoods for the original and modified PI and RI

Table 3
Contingency table for $w=0.25$ for the modified PI and RI forecasts in (a) and (b), respectively

Forecast	Observed		
	Yes	No	Total
a. PI, $w=0.25$			
Yes	(a_{SUM}) $1\times78+0\times19=78$	(b_{SUM}) $45\times78+46\times19=4384$	4462
No	(c_{SUM}) $0\times78+1\times19=19$	(d_{SUM}) $2954\times78+2953\times19=286,519$	286,538
Total	97	290,903	291,000
b. RI, $w=0.25$			
Yes	(a_{SUM}) $1\times49+0\times48=49$	(b_{SUM}) $45\times49+46\times48=4413$	4462
No	(c_{SUM}) $0\times49+1\times48=48$	(d_{SUM}) $2954\times49+2953\times48=286,490$	286,538
Total	97	290,903	291,000

forecasts are computed and the results are given in Fig. 3b. The value of $\log_{10}(L_P)$ for the modified PI is larger than those of the other log-likelihoods. We compute the log-likelihoods for the RAN forecast obtained by applying the modified PI method to 100 random catalogs. The results are shown in this figure (histogram). Since larger values of the log-likelihoods indicate a more successful hypothesis, the logical conclusion is that the modified PI technique has better forecast skill relative to the original PI technique, the original and modified RI techniques, and the RAN forecast technique.

6. Correspondence of the forecast with the data

To test a forecast (or hypothesis) against a null hypothesis is a necessary step for evaluation of a hypothesis. However, we should also test the correspondence of the forecast with the data. These tests, in the framework of likelihood testing, has been proposed by many researchers (e.g., Kagan and Jackson, 1991, 1994, 1995; Jackson, 1996; Kagan and Jackson, 2000; Schorlemmer et al., 2006). Without showing that the forecast corresponds to the observation, we should not claim a successful forecast. Applying only the likelihood test does not allow a statement of quality. Although the spatial distribution of earthquakes denoted by circles seems to agree with that of the seismically anomalous regions, we want to quantitatively assess the effectiveness of the forecast in Fig. 1c. How do we evaluate the statistical significance of a seismic hazard map? The question was highlighted by Kagan and Jackson (1991) in their discussion of the seismic gap hypothesis. In this paper, following Kagan and Jackson (1994), we use a variant of the bootstrap technique based on Monte Carlo simulations (see also Kagan and Jackson, 2000). We first simulate earthquake sequences using the forecast map in Fig. 1c. Then, we compare the log-likelihoods for these synthetic catalogs, $\log_{10}(L_{G,k})$ for the Gaussian model and $\log_{10}(L_{P,k})$ for the Poissonian model, with those for the control catalog that is the catalog of earthquakes indicated by circles in Fig. 1c, $\log_{10}(L_G)=-182$ and $\log_{10}(L_P)=-208$, respectively. Note that $\log_{10}(L_{G,k})$ and $\log_{10}(L_{P,k})$ are the log-likelihoods for the earthquake sequence obtained by the k-th simulation with $k=1, 2,\ldots, N_{SIM}$, where N_{SIM} is the total number of simulations. The distribution of these log-likelihoods is normal (Gaussian) for large N_{SIM}.

For our case, synthetic catalogs of 97 earthquakes are made based on the forecast map in Fig. 1c. We use the rejection method for generating random deviates (Press et al., 1992, p. 290) to distribute these earthquakes. The brief description of how this method is applied to making a synthetic catalog is given below. At the first step, choose a point randomly from any point in the study region. Second, generate a random number (0 to 1). Here there are two realizations. 1) If this random number is larger than the PI score for the box into which the random point is included, this point is rejected and we do not take the point into consideration. Then, we go back to the first step. 2) If it is smaller than the PI score, this random point is accepted and we assume that an earthquake occurs at this point in the forecast interval. We include this earthquake into the synthetic catalog and then go back to the first step. This procedure is repeated until 97 earthquakes are included into the

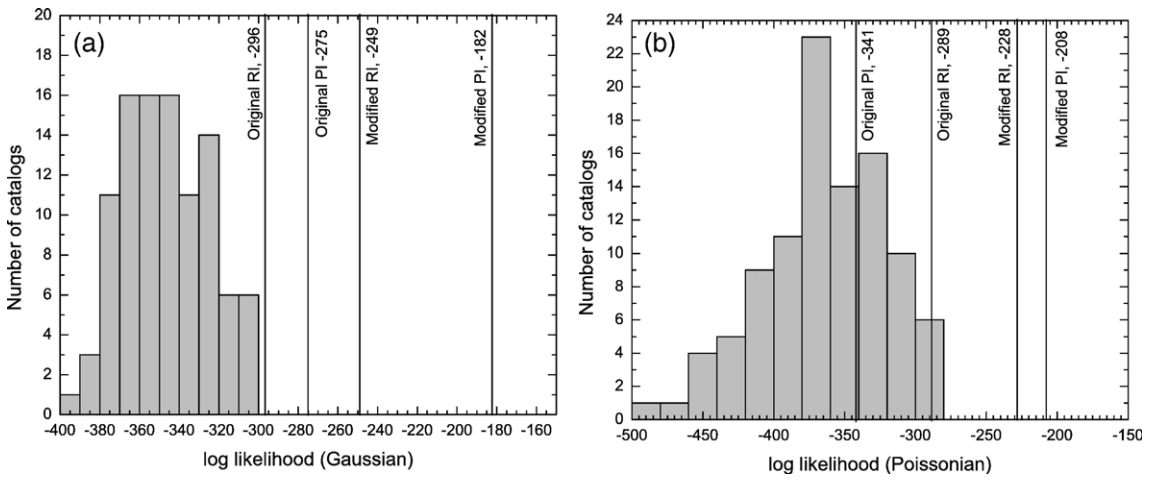

Fig. 3. Plots of log-likelihoods for 100 random catalogs (histogram); for the use of the original and modified RI forecasts; and for the use of the original and modified PI forecasts. (a) Global Gaussian model and (b) local Poissonian model.

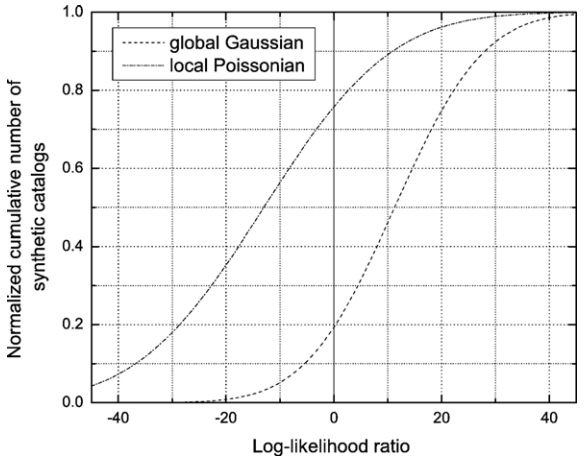

Fig. 4. Testing the forecast in Fig. 1c. We use the 2000–2009 earthquakes as a control set. The bootstrap distribution is given by the dashed curve for the use of the Gaussian model and by the dash-dotted curve for the use of the Poissonian model. The mean and standard deviation calculated based on the 1000 realizations are 11.29 and 13.05 for the Gaussian model, respectively. For the same realizations, we obtain the mean of −12.98 and the standard deviation of 18.60 for the Poissonian model. Computed data on the left of the vertical solid line are constituted of simulations worse than the real earthquake distribution (the control set); curves on the right are constituted of simulation better than the real earthquake distribution.

catalog. We made $N_{\mathrm{SIM}}=1000$ synthetic catalogs to assess the effectiveness of the forecast in Fig. 1c.

Fig. 4 shows bootstrap distributions. Normalized cumulative number of synthetic catalogs is given as a function of the log-likelihood ratios defined by $\log_{10}(L_{\mathrm{G}}/L_{\mathrm{G},k})$ and $\log_{10}(L_{\mathrm{P}}/L_{\mathrm{P},k})$. This normalization means that cumulative number of catalogs is divided by N_{SIM}. That is, this normalized number is from 0 to 1. Following Kagan and Jackson (1994), we consider that the forecast is rejected if the observed (that is, test or control) catalog is too different from the simulated catalogs (that is, if $\log_{10}(L_{\mathrm{G}}/L_{\mathrm{G},k})=0$ and $\log_{10}(L_{\mathrm{P}}/L_{\mathrm{P},k})=0$ fall within upper or lower 5% of the cumulative distribution). As shown in Fig. 4, the normalized number of catalogs is 0.19 at $\log_{10}(L_{\mathrm{G}}/L_{\mathrm{G},k})=0$ and 0.76 at $\log_{10}(L_{\mathrm{P}}/L_{\mathrm{P},k})=0$. That is to say, the observed catalog does not fall within upper or lower 5% of the cumulative distribution. This result shows that the observed catalog is consistent with the simulated catalogs. Thus, our forecast is acceptable.

One may note that Schorlemmer et al. (2006) studied the technique of Kagan and Jackson (1994, 2000) in depth for California earthquakes. We agree that the use of the technique adopted in our paper is a preliminary step and a detailed investigation to support our result obtained here would require the use of the technique of Schorlemmer et al. (2006).

7. Seismic activation and quiescence

As shown in the step 8 of the PI forecast algorithm described in Section 2.2, we square $\Delta\underline{n}_i^*(t_0,t_1,t_2)$ in order to obtain the probability in box i, $P_i(t_0,t_1,t_2)$. This probability is a measure of both seismic activation and quiescence. The area of $\Delta\underline{n}_i^*(t_0,t_1,t_2)>0$ is the area that has experienced seismic activation in the change interval t_1 to t_2. Similarly, the area of $\Delta\underline{n}_i^*(t_0,t_1,t_2)<0$ is the area that has experienced seismic quiescence in the change interval t_1 to t_2. Here we distinguish between the areas of the seismic activation and quiescence. Two color-codes, red and blue, are used to express the logarithmic values of PI score $\log_{10}$(PI score) when the $\Delta\underline{n}_i^*(t_0,t_1,t_2)>0$ and those when $\Delta\underline{n}_i^*(t_0,t_1,t_2)<0$, respectively. The result is shown in Fig. 5. The times (t_0, t_1, t_2) used for this figure are the same as those used for Fig. 1c. We see both blue and red areas in this figure. Circles are the earthquakes of $m_{\mathrm{JMA}}\geq 5$ since 2000. The area associated with the 2004 Niigata earthquake has experienced seismic activation prior to the occurrence of this earthquake. The area associated with the 2000

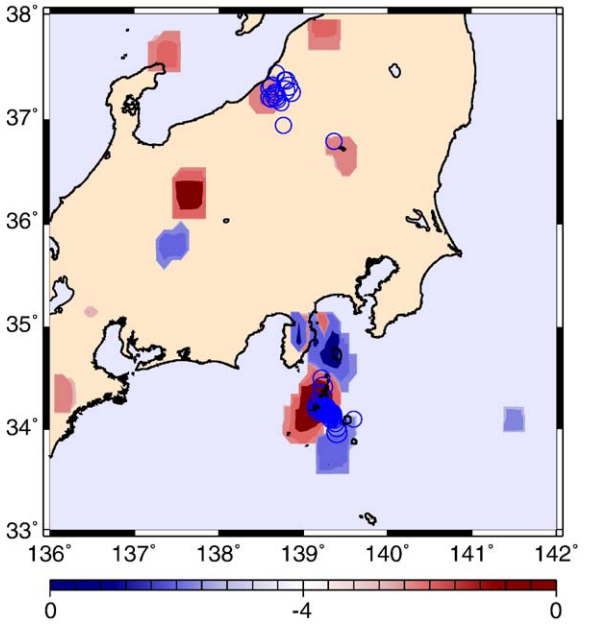

Fig. 5. PI forecast map with two color-codes. Logarithmic values of the PI score $\log_{10}$(PI score) are given using the blue color-code when $\Delta\underline{n}_i^*(t_0,t_1,t_2)<0$ and using the red color-code when $\Delta\underline{n}_i^*(t_0,t_1,t_2)>0$. The times used are t_0=Jan. 1, 1965, t_1=Jan. 1, 1990, and t_2=Dec. 31, 1999. The areas in red and blue has experienced the seismic activation and quiescence, respectively, in the change interval from t_1 to t_2. Circles in this figure are earthquakes that occurred in the forecast interval for the magnitude $5.0\leq m_{\mathrm{JMA}}$. Details of the correspondence between the color bar and the colors used in the figure and coloring the offshore and onshore regions are given in the caption of Fig. 1.

Miyake earthquake swarm has experienced both seismic activation and quiescence prior to the occurrence of this swarm.

We confirm that red and blue areas have experienced seismic activation and quiescence, respectively. An approach to doing this is to make the graph of the cumulative number of earthquakes N_{CUM} as a function of time t. This approach has been taken to detect precursory seismic quiescence (e.g., Habermann, 1988; Wyss and Habermann, 1988). For instance, Fig. 6a shows the results for the area associated with the 2004 Niigata earthquake since the time t_0 = Jan. 1, 1965. This area is between 37.0 and 37.4° north latitude and between 138.4 and 138.8° east longitude. Also included into this figure are two regression lines fitted to the data in the periods t_0 to t_1 (dashed line) and t_1 to t_2 (solid line). The slopes of the regression lines show that the number of earthquakes per year is about one during the period t_0 to t_1 and about three during the period t_1 to t_2. This shows that the rate of seismic activity for the former period is lower than that for the latter period, confirming the suggestion of seismic activation in this area. The same procedure has been performed for other anomalous areas shown in Fig. 5. The results for the two areas of seismic quiescence and activation associated with the 2000 Miyake earthquake swarm are shown in

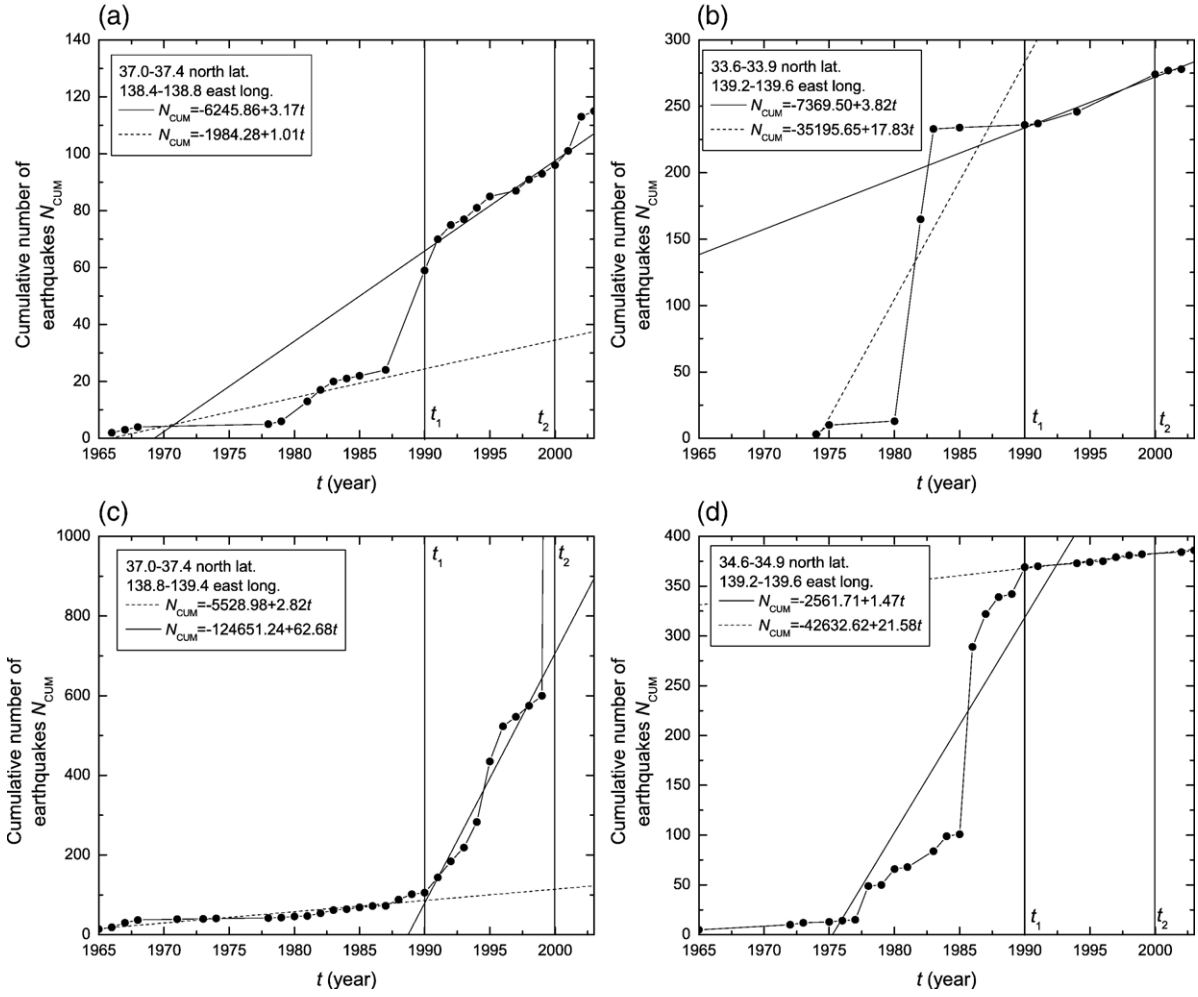

Fig. 6. Cumulative number of earthquakes per year N_{CUM} as a function of time t (year) for the four areas: (a) The area between 37.0–37.4° north latitude and between 138.4–138.8° east longitude, (b) the area between 33.6–33.9° north latitude and between 139.2–139.6° east longitude, (c) the area between 37.0–37.4° north latitude and between 138.8–139.4° east longitude, and (d) the area between 34.6–34.9° north latitude and between 139.2–139.6° east longitude. The area shown in (a) is associated with the anomaly of the 2004 Niigata earthquake. The areas for (b) and (c) are associated with the anomalies of the 2000 Miyake earthquake swarm. The area for (d) has experienced the strongest seismic quiescence in the study region. Vertical lines denote the times t_1 = Jan. 1, 1990 and t_2 = Dec. 31, 1999. Also included are the regression lines fitted to the data in the range t_1 to t_2 (solid line) and the range t_0 to t_1 (dashed line).

Figs. 6b and c, respectively. Fig. 6d shows the result for the area that has experienced the strongest seismic quiescence in the map (between 34.6 and 34.9° north latitude and between 139.2 and 139.6°). We confirm that clear seismic activation or quiescence in each figure.

8. Discussion

If the observed spatial pattern of the anomaly in Fig. 1c were largely changed for varying the time t_0, then discussion based on this figure would be questionable. To test this idea, we took the time t_0 to be Jan. 1, 1940 to Jan. 1, 1988 to generate the PI forecast maps. The times t_1, t_2, and t_3 are the same as those defined in Section 4. To statistically check this, we use the log-likelihood ratio in Fig. 7. This ratio is defined by the subtraction of $\log_{10}(L_G)$ and $\log_{10}(L_P)$ for the time t_0 given at the horizontal axis from $\log_{10}(L_G)$ and $\log_{10}(L_P)$ for the reference time t_0=Jan. 1, 1965, respectively. We see that the ratios do not vary for t_0=1940–1970 and the smallest values for both Gaussian and Poissonian models are given for t_0=1965. The ratio increases after t_0=1983 for the Gaussian model and after t_0=1975 for the Poissonian model. Also used are the Molchan and ROC diagrams as done above and it is generally seen that the curves for t_0=1940–1970 (not shown) are not different from the curve t_0=1965 in Figs. 2a and b (solid curve in red). The maps for t_0=1940–1970 are not significantly different so that we do not show them.

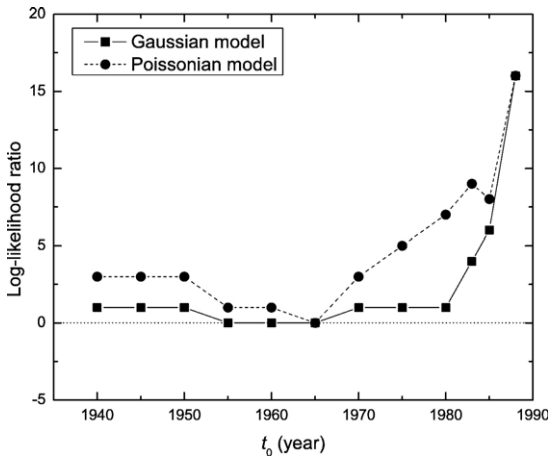

Fig. 7. Forecast performance as a function of t_0 (year) in terms of the Gaussian (solid curve) and Poissonian (dashed curve) models. The log-likelihood ratio is defined by the subtraction of $\log_{10}(L_G)$ and $\log_{10}(L_P)$ for the time t_0 given at the horizontal axis from $\log_{10}(L_G)$ and $\log_{10}(L_P)$ for the reference time t_0=Jan. 1, 1965, respectively. The times t_1, t_2, and t_3 are the same as those defined in Section 4. The values above the horizontal dotted line represent the performance worse than that for the reference time.

These tests show that the spatial pattern of the anomaly is stable for variations of the time t_0 within the range t_0=1940–1970, so discussion based on Fig. 1c with t_0=Jan. 1, 1965 is not so questionable. However, note that according to our knowledge, completeness of the JMA earthquake data does not exist since 1965.

In this paper, testing a forecast against data containing many events from essentially two swarms, the Niigata and Miyake swarms, may not be an appropriate setup to measure the performance of the PI forecast. Thus, it is of interest to remove, at least, the aftershock sequence of the Niigata earthquake from our analysis. Here we do this and apply the modified PI and RI methods to competing the forecasts based on these methods. We compute the log-likelihoods for the Gaussian model so that the obtained values are $\log_{10}(L_G)=-138$ for the modified PI and $\log_{10}(L_G)=-202$ for the modified RI. Next we take the Poissonian model. The log-likelihoods obtained are $\log_{10}(L_P)=-172$ for the modified PI, and $\log_{10}(L_P)=-200$ for the modified RI. For both models, the log-likelihood for the PI forecast is larger than that for the RI forecast. We compute the performance of the PI and RI forecasts according to the Molchan and ROC diagrams and include the results into Figs. 2a and b. The solid and dashed curves in cyan color correspond to the use of the modified PI and RI methods, respectively. For both diagrams, it is generally seen that the curve of the PI forecast is located in the upper left relative to that of the RI forecast. Thus, the result obtained here is that the modified PI technique has better forecast skill relative to the modified RI one even if the aftershock sequence of the Niigata earthquake is removed from our analysis. This leads to further support our primary conclusion.

9. Summary and conclusions

Recently, our group developed a new approach to earthquake forecasting. This approach is based on a Pattern Informatics (PI) algorithm, which can be used to detect seismic activation and quiescence and to make earthquake forecasts (Rundle et al., 2002, 2003; Tiampo et al., 2002). The objective is to narrow the possible locations where large earthquakes are expected to occur in the near future (from a few to as many as ten years). This approach has been applied to California, Japan and on a worldwide basis (e.g., Holliday et al., 2005). In this paper we modified the original PI method and applied this to forecasting future (2000–2009) large ($m_{JMA} \geq 5$) earthquakes in the central part of Japan (33–38° north latitude, 136–142° east longitude). This modification is an introduction of the idea of Moore neighborhood into

the process to construct PI forecast. We visually compared between the hazard maps made by using the original and modified PI methods. We paid attention to the association of the large earthquakes in the forecast interval (2000–2009) with the possible locations where large earthquakes are expected. We found that this association for the modified PI method is stronger than that for the original PI method. The modified approach enlarges the areas of the possible location with high PI values and reduces "noisy" anomalies that are the areas with small PI values. To objectively test whether or not this modification is effective, we adopted three statistical methods, the Molchan and ROC diagrams and the log-likelihood test. For all tests it was seen in general that the modified-PI-based forecast performs significantly better than the original-PI-based forecast and the forecasts based on the two null hypotheses (RI method and RAN method). We further examine our modified-PI forecast by using the bootstrap test in order to check the correspondence of its forecast to the data. This examination showed the result that our forecast is statistically acceptable for the correspondence to the data. To show this applicability of our new method to forecasting earthquakes beyond doubt, we distinguished the areas of seismic anomaly into two areas of seismic activation and quiescence and confirmed that these observed areas did indeed demonstrate activation and quiescence, by plotting the cumulative number of earthquakes per year as a function of time (year) for several areas of seismic anomaly. The modification presented in this paper is one of our innovative and state-of-the-art sciences that Nanjo et al. (in press) did not do. It will be of interest to understand how this new PI approach can be applied to other regions, especially tectonically active and complex regions such as Taiwan (Chen et al., 2005). Our results indicate that the modified PI method shows considerable promise as an intermediate-term earthquake forecasting tool.

Further investigation discussed below makes an interesting contribution to the understanding of the applicability of the (modified or original) PI method to forecasting earthquakes. The analysis given in this paper is for a two-dimensional problem. It is desirable to extend the analysis to a fully three-dimensional (3D) forecast. One way to do this is to generate a 3D forecast map. We claim that further investigation of this approach would help us to understand earthquake forecasting in a 3D subduction zone where an oceanic plate is subducting beneath a continental plate, such as subduction of the Pacific plate under the eastern margin of the Eurasian plate.

Finally, some readers may see little value in testing a forecast issued for the period 2000–2009. So far, only half of this period has passed and any evaluation of the described forecast may be regarded as preliminary. Additionally, it may be felt that the method presented does not have adequate a posteriori justification. One approach to support the effectiveness of the modified PI method would be to perform the same procedure for a different, previous decade, e.g., 1990–1999 and to demonstrate that the applied strategy would be able to correctly identify the large events that occurred in the past. This would allow us to "tune" this strategy and give at least an empirical explanation about the choices. Thus, demonstrating that it could be efficiently applied in an a posteriori manner in the past will be our next research. It will allow the potential readers to learn something about the method and its applicability to an important seismicity region such as Japan.

Acknowledgement

We are grateful to the two anonymous reviewers and the guest editor G. Zöller for their helpful remarks which significantly improved the manuscript. DLT acknowledges NSF grant ATM-03-27571. Research by JBR is funded by DOE/OBES grant DE-FG03-95ER14499 (theory), by NASA grant NAG5-5168 (simulations), and by the Southern California Earthquake Center. CCC is grateful for the research support from the National Science Council (ROC) and the Department of Earth Sciences (NCU-ROC). JRH is supported by the NASA Earth System Science Fellowship. KZN thanks Y. Ogata, S. Toda, T. Iwata, B. Enescu, and H. Tsuruoka for valuable comments and JMA for providing Japanese earthquake data. Also, research by KZN is supported by JSPS Research Fellowship; Grant-in-Aid 17200021 for Scientific Research, The Ministry of Education, Culture, Sport, Science and Technology; and Transdisciplinary Research Integration Center, Research Organization of Information and Systems. Figs. 1 and 5 are generated using the GMT software (Wessel and Smith, 1998).

References

Bevington, P.R., Robinson, D.K., 1992. Data Reduction and Error Analysis for the Physics Sciences, 2nd ed. McGraw-Hill, New York. 328 pp.

Bowman, D.D., Ouillon, G., Sammis, C.G., Sornette, A., Sornette, D., 1998. An observational test of the critical earthquake concept. J. Geophys. Res. 103, 24359–24372.

Bufe, C.G., Varnes, D.J., 1993. Predictive modeling of the seismic cycle of the greater San Francisco Bay region. J. Geophys. Res. 98, 9871–9883.

Chen, C.-c., Rundle, J.B., Holliday, J.R., Nanjo, K.Z., Turcotte, D.L., Li, S.-c., Tiampo, K.F., 2005. The 1999 Chi-Chi, Taiwan, earthquake as a typical example of seismic activation and quiescence. Geophys. Res. Lett. 32 (22), L22315.

Du, W.X., Sykes, L.R., 2001. Changes in frequency of moderate-size earthquakes and coulomb failure stress before and after the Landers, California, earthquake of 1992. Bull. Seismol. Soc. Am. 91, 725–738.

Enescu, B., Ito, K., 2001. Some premonitory phenomena of the 1995 Hyogo-Ken Nanbu (Kobe) earthquake: seismicity, *b*-value and fractal dimension. Tectonophysics 338, 297–314.

Gross, S., Rundle, J.B., 1998. A systematic test of time-to-failure analysis. Geophys. J. Int. 133, 57–64.

Habermann, R.E., 1988. Precursory seismic quiescence: past, present, and future. Pure Appl. Geophys. 126, 279–318.

Holliday, J.R., Nanjo, K.Z., Tiampo, K.F., Rundle, J.B., Turcotte, D.L., 2005. Earthquake forecasting and its verification. Nonlinear Process. Geophys. 12, 965–977.

Jackson, D.D., 1996. Hypothesis testing and earthquake prediction. Proc. Natl. Acad. Sci. U. S. A. 93, 3772–3775.

Jaumè, S.C., Sykes, L.R., 1999. Evolving towards a critical point: a review of accelerating seismic moment/energy release prior to large and great earthquakes. Pure Appl. Geophys. 155, 279–306.

Joliffe, I.T., Stephenson, D.B. (Eds.), 2003. Forecast Verification: A Practitioner's Guide in Atmospheric Science. John Wiley and Sons, England. 254 pp.

Kagan, Y.Y., Jackson, D., 1991. Seismic gap hypothesis: ten years after. J. Geophys. Res. 96, 21,419–21,431.

Kagan, Y.Y., Jackson, D., 1994. Long-term probabilistic forecasting of earthquakes. J. Geophys. Res. 99, 13,685–13,700.

Kagan, Y.Y., Jackson, D., 1995. New seismic gap hypothesis: five years after. J. Geophys. Res. 100, 3943–3959.

Kagan, Y.Y., Jackson, D., 2000. Probabilistic forecasting of earthquakes. Geophys. J. Int. 143, 438–453.

Kanamori, H., 2003. Earthquake prediction: an overview. In: Lee, W. H.K., Kanamori, H., Jennings, P.C., Kisslinger, C. (Eds.), International Handbook of Earthquake and Engineering Seismology. Academic Press, Amsterdam, pp. 1205–1216.

Kellis-Borok, V.I., 1990. The lithosphere of the Earth as a nonlinear system with implications for earthquake prediction. Rev. Geophys. 28, 19–34.

Kellis-Borok, V.I., Kossobokov, V.G., 1990. Premonitory activation of earthquake flow: algorithm M8. Phys. Earth Planet. Inter. 61, 73–83.

Kellis-Borok, V.I., Rotwain, I.M., 1990. Diagnosis of time of increased probability of strong earthquakes in different regions of the world. Phys. Earth Planet. Inter. 61, 57–72.

Kellis-Borok, V.I., Soleviev, A.A. (Eds.), 2003. Nonlinear Dynamics of the Lithosphere and Earthquake Prediction. Springer-Verlag, New York. 341 pp.

Main, I.G., 1999. Applicability of time-to-failure analysis to accelerated strain before earthquakes and volcanic eruptions. Geophys. J. Int. 139, F1–F6.

Matthews, M.V., Reasenberg, P., 1987. Comment on Habermann's method for detecting seismicity rate changes. J. Geophys. Res. 92 (B9), 9443–9450.

McGuire, J.J., Boettcher, M.S., Jordan, T.H., 2005. Foreshock sequences and short-term earthquake predictability on East Pacific Rise transform faults. Nature 434, 457–461.

Mogi, K., 1985. Earthquake Prediction. Academic Press, Tokyo. 355 pp.

Molchan, G.M., 1997. Earthquake prediction as a decision-making problem. Pure Appl. Geophys. 149, 233–247.

Nanjo, K.Z., Rundle, J.B., Holliday, J.R., Turcotte, D.L., in press. Pattern informatics and its application for optimal forecasting of large earthquakes in Japan, Pure Appl. Geophys.

Newman, W.I., Turcotte, D.L., 2002. A simple model for the earthquake cycle combining self-organized complexity with critical point behavior. Nonlinear Process. Geophys. 9, 453–461.

Papazachos, C.B., Karakaisis, G.F., Scordilis, E.M., Papazachos, B.C., 2005. Global observational properties of the critical earthquake model. Bull. Seismol. Soc. Am. 95, 1841–1855.

Press, W.H., Teukolsky, S.A., Vetterling, W.T., Flannery, B.P., 1992. Numerical Recipes in C: The Art of Scientific Computing, 2nd ed. Cambridge Univ. Press, New York. 994 pp.

Rundle, J.B., Tiampo, K.F., Klein, W., Martins, J.S.S., 2002. Self-organization in leaky threshold systems: the influence of near-mean field dynamics and its implications for earthquakes, neurobiology, and forecasting. Proc. Natl. Acad. Sci. U. S. A. 99, 2514–2521.

Rundle, J.B., Turcotte, D.L., Shcherbakov, R., Klein, W., Sammis, C., 2003. Statistical physics approach to understanding the multiscale dynamics of earthquake fault systems. Rev. Geophys. 41 (4), 1019. doi:10.1029/2003RG000135.

Scholz, C.H., 2002. The Mechanics of Earthquakes and Faulting, 2nd ed. Cambridge Univ. Press, New York. 471 pp.

Schorlemmer, D., Gerstenberger, M., Wiemer, S., Jackson, D.D., 2006. Earthquake likelihood model testing, http://www.earthquake.ethz.ch/docs/drafts/draft_relmtest.

Scordilis, E.M., 2005. Globally valid relations converting Ms, m_b and M_{JMA} to Mw. In: Husebye, E.S., Christova, C. (Eds.), Book of Abstracts of NATO Advanced Research Workshop, Earthquake Monitoring and Seismic Hazard Mitigation in Balkan Countries. Kamea Ltd., Sofia, pp. 158–161.

Sykes, L.R., Jaumè, S.C., 1990. Seismic activity on neighboring faults as a long-term precursor to large earthquakes in the San Francisco area. Nature 348, 595–599.

Tiampo, K.F., Rundle, J.B., McGinnis, S., Gross, S.J., Klein, W., 2002. Mean field threshold systems and phase dynamics: an application to earthquake fault systems. Europhys. Lett. 60, 481–487.

Turcotte, D.L., 1991. Earthquake prediction. Annu. Rev. Earth Planet. Sci. 19, 263–281.

Turcotte, D.L., 1997. Fractals and Chaos in Geology and Geophysics. Cambridge Univ. Press, New York. 398 pp.

Wells, D.L., Coppersmith, K.J., 1994. New empirical relationships among magnitude, rupture length, rupture area and surface displacement. Bull. Seismol. Soc. Am. 84, 974–1002.

Wessel, P., Smith, W.H.F., 1998. New, improved version of the Generic Mapping Tool released. EOS Trans. AGU 79, 579.

Wolfram, S., 2002. A New Kind of Science. Wolfram Media, Champaign, IL. 1197 pp.

Wyss, M., 1997. Nomination of precursory seismic quiescence as a significant precursor. Pure Appl. Geophys. 149, 79–114.

Wyss, M., Habermann, R.E., 1988. Precursory quiescence before the August 1982 Stone Canyon, San Andreas Fault, earthquakes. Pure Appl. Geophys. 126 (2–4), 333–356.

Wyss, M., Martirosyan, A.H., 1998. Seismic quiescence before the M 7 1988 Spitak earthquake, Armenia. Geophys. J. Int. 134, 329–340.

Wyss, M., Wiemer, S., 2000. Change in the probability for earthquakes in southern California due to the Landers magnitude 7.3 earthquake. Science 290, 1334–1338.

Zöller, G., Hainzl, S., Kurths, J., 2001. Observation of growing correlation length as an indicator for critical point behavior prior to large earthquakes. J. Geophys. Res. 106, 2167–2176.